Role of interface potential barrier, Auger recombination and temporal coherence in $In_{0.5}Ga_{0.5}As$/GaAs Quantum Dots based p-i-n light emitting diodes

Mohit Kumar Singh[1], Amit Bhunia[1], Maryam Al Huwayz[2,5],

Y. Galvão Gobato[3,4], Mohamed Henini[5,6] and Shouvik Datta[1] *

[1]Department of Physics & Centre for Energy Science, Indian Institute of Science Education and Research, Pune 411008, Maharashtra, India

[2]Department of Physics, College of Sciences, Princess Nourah bint Abdulrahman University (PNU), Riyadh 11671, Saudi Arabia

[3]Departamento de Física, Universidade Federal de São Carlos, 13560-905, São Carlos, SP, Brazil

[4]High Field Magnet Laboratory (HFML-EMFL), Radboud University, 6525 ED Nijmegen, Netherlands

[5]School of Physics and Astronomy, University of Nottingham, Nottingham NG7 2RD, UK

[6]UNESCO-UNISA Africa Chair in Nanosciences & Nanotechnology Laboratories, College of Graduate Studies, University of South Africa (UNISA), Muckleneuk Ridge, PO Box 392, Pretoria, South Africa

***Corresponding author's email:** shouvik@iiserpune.ac.in

Abstract

In this work, we investigate the mechanisms that control the electroluminescence from p-i-n heterostructures containing self-assembled $In_{0.5}Ga_{0.5}As$ quantum dots embedded inside $GaAs/Al_{0.3}Ga_{0.7}As$ quantum well as a function of temperature and applied bias. Our results reveal that the carrier dynamics at the interface between the quantum dot and the quantum well plays a crucial role in the electroluminescence emission. At low temperatures, two distinct emission bands are observed. Initially at low bias current, we observe broad emissions from quantum well and wetting layers. Another dominant and sharp emission at lower energy arises from the quantum dots but only at higher bias currents. We discuss how a potential barrier between quantum dots and quantum well can control the density of injected carriers undergoing optical recombination. We have also investigated the role of carrier capture and escape, quantum-confined stark effect, and band filling effects in the electroluminescence emission. In addition, we demonstrate how measurements of temporal coherence of individual spectral peaks, can detect the presence of Auger recombination in quantum dots under high injection currents. Interestingly, a significant increase in temporal coherence of quantum dot emissions is observed, which could be due to a decrease in Auger recombination with increasing temperature.

Keywords: Quantum Dots, Electroluminescence, Coherence, Auger recombination

(All figures may appear in colour only in the online journal)

1. Introduction

Quantum dot (QD) laser is a device of great interest in optoelectronics because of its expected energy efficiency [1], temperature stability, and spectral sharpness, which can be better than existing quantum well (QW) lasers [2]. Three-dimensional spatial confinement and atom like sharp density of states in QD are the reasons for its low lasing threshold and narrow emission spectra [3-5]. Through improvements in material engineering, growth techniques and device level structural modification, QD lasers are getting more efficient and applicable for various technologies [6-8]. One such modification for extra confinement of charge carriers is embedding quantum dots within quantum well (QD-QW) system [9, 10]. Such step-by-step like band structure improves the carrier confinement inside the quantum dots and as a result, improves the light emission [11-13]. However, internal potential barriers can be formed at the interface of such heterostructures, which can significantly affect the carrier transport and electroluminescence inside a QD-QW. Also, the energy levels of QDs, which depend on size and mole fractions of alloy materials, determine the extent of thermal escape and capture of carriers from QDs and luminescence quenching [10, 14]. Usually, the physics of excitonic recombination [15], non-radiative defects [16], thermal escape and re-capture [17], Auger recombination [18] etc were previously explored to explain the outcome of these QD lasers. Numerous electrical and optical investigations were also reported showing how these can affect QDs emission. However, there is still hardly any consensus on the interpretation of these findings. Specifically, the role of interface potential and its effect on electroluminescence spectra and temporal coherence are rarely discussed in the literature. Therefore, detailed investigations of all these aforementioned factors can be utilized to overcome some generic problems of QD laser diodes such as inability of high power emissions, efficiency droop [19] etc.

In this paper, we present an investigation on the opto-electrical properties as a function of applied bias and temperature of an $In_{0.5}Ga_{0.5}As/GaAs/Al_{0.3}Ga_{0.7}As$ QD-QW p-i-n heterostructure. We use two similar samples with and without distributed Bragg reflector (DBR) stacks. Most of these studies are done on the latter sample without any DBR and the first sample is used only for comparison purposes. Detailed descriptions of both samples and experimental setups are given in section 2. We observe two distinct electroluminescence (EL) peaks at ~8.8 K: one from QDs and the other from QWs and wetting layer (WL) combined. In the low current density regime, evolution of both peaks with increasing bias currents are analysed. We discuss how the potential barrier formed at the interface of QD and QW can

play an important role. Dependence of bias current and temperature of EL spectra are discussed in details in section 3 for samples without DBR and it is compared with the other sample. Also in the same section, the temporal coherence of the EL of sample without DBR is analysed in the high current density regime using a Michelson interferometer. Thereby, we explain how Auger recombination (AR) affects optical coherence of the EL from the $In_{0.5}Ga_{0.5}As$ QDs in high bias current regime. Surprisingly, the temporal coherence of QD emission increases with increasing temperature.

2. Samples and Experimental Methods

The two samples investigated here were grown by Molecular Beam Epitaxy (MBE) on semi-insulating GaAs (100) substrates. Sample A is a p-i-n heterostructure with QDs embedded within a QW. A buffer layer of 500 nm of n-type GaAs ($6\times10^{18}/cm^3$) was grown on the substrate at 600°C, which serves as n-type bottom electrical contact for the sample. It is followed by 800 Å of $Al_{0.3}Ga_{0.7}As$ and six layers of QD-QW system. The central of QD-QW structure, which was grown at 450 °C, consisted of 100 Å of $Al_{0.3}Ga_{0.7}As$, 51 Å of GaAs, 11 Å $In_{0.5}Ga_{0.5}As$ and 51 Å of GaAs. This way $In_{0.5}Ga_{0.5}As$ quantum dots were grown inside ~100Å GaAs/$Al_{0.3}Ga_{0.7}As$ QW. This was followed by 800 Å $Al_{0.3}Ga_{0.7}As$ layer. Finally, the structure is capped with 1.3 μm of highly doped p-type $Al_{0.6}Ga_{0.4}As$/GaAs ($6\times10^{18}/cm^3$) for top electrical contact. Ring shaped mesas of diameter ~400 μm and area of ~$5x10^{-4}$ cm^2 were made with gold for both optical and electrical access from the top. For sample B, the 3 key differences over sample A are – (i) there are three layers of QD-QW system instead of six (as in sample A), (ii) the 800 Å $Al_{0.3}Ga_{0.7}As$ layer above and below the QD-QW layers are replaced by 1100 Å $Al_{0.3}Ga_{0.7}As$ layer, (iii) 20 repetitions of $Al_{0.6}Ga_{0.4}As$ (18 Å) and GaAs (10 Å) were deposited at 600°C on either side of this active structure which works as DBR cavity.

Samples are kept within customized copper sample holder inside ARS CS204-DMX-20 closed cycle cryostat for temperature dependent measurements. The electrical bias is applied using Agilent's E4980A LCR meter in DC mode. EL spectra are measured with CCS200 spectrometer from Thorlabs. Spectral bandwidth of the spectrometer is kept < 2 nm (@ 633 nm) unless specified otherwise. EL was measured under forward bias levels above which the device capacitance (30 mV, 1 kHz) goes to negative [20, 21]. The λ^2 correction was

incorporated in all EL spectra presented here. We want to further clarify that bias currents range for spectral studies in section 3.1 is from 0.11 mA to 2.2 mA.

Measurements of temporal coherence are done using a piezo controlled Michelson Interferometer. Light coming from samples is first focused on a 50:50 beam splitter. Distance between mirrors and beam splitter is used to create a temporal lag (τ) between the two split beams. These temporally separated beams are then superimposed to create interference pattern whose visibility determines the magnitude of temporal coherence e.g. magnitude of first order correlation function $g^{(1)}(\tau)$. One of the interferometer arm is controlled by a Piezo controller having a minimum spatial resolution of 20 nm and other arm is controlled by a stepper motor having a resolution of 10 μm. Position of mirrors are optimized to be at equal length from beam splitter to measure autocorrelation function $g^{(1)}(\tau=0)$. Output of the interferometer is fed to Acton Research's SP2555i monochromator with a full spectral bandwidth of 9.6 nm to separate the interference patterns arising out of two different spectral regions. Interference patterns are finally recorded with Thorlabs BC106N-VIS/M CCD camera. For coherence studies, we have used bias currents from 1 mA to 15 mA.

3. Experimental Results.

3.1 Bias dependence of electroluminescence from QD and QW-WL

Figure 1 shows the EL spectra measured at ~8.8 K with varying levels of forward bias. Decreasing values of forward bias voltages and corresponding currents are indicated inside figure 1(a), (b) and (c), respectively. We clearly see two distinct bands: one around 1.33 eV due to the EL from the $In_{0.5}Ga_{0.5}As$ QDs and another one around 1.47 eV due to the GaAs/$Al_{0.3}Ga_{0.7}As$ QW and $In_{0.5}Ga_{0.5}As$ wetting layer. From now on, we will refer to the emission at 1.47 eV as QW-WL emission as it also has the contributions of QD wetting layers. It is evident from figure 1(c) that at low bias currents, the emission of the QW-WL peak is more prominent than the actual $In_{0.5}Ga_{0.5}As$ QD peak. It can be seen from the contour diagram in figure 1(d) that even the emission of QW-WL starts before the QD emission. The QD peak begins to show up only after a bias current of ~0.33 mA. This implies that after initial injection of carriers, the first major radiative recombination happens inside QW-WL, not at QD. However, at higher bias currents, intensity of these QD peaks increase substantially as compared to the QW-WL peaks.

In order to understand the above-mentioned observations, we draw a schematic of the QD-QW heterostructure sample and its potential landscape in figure 2(a) and 2(b), respectively. The gray shadow over QDs in figure 2(a) and inset of figure 2(b) indicates the presence of a potential barrier at $In_{0.5}Ga_{0.5}As/GaAs$ interface [9, 22-24] of the conduction band. This is likely to be created by the transfer of electrons from the higher lying GaAs conduction band to low potential regions of $In_{0.5}Ga_{0.5}As$ conduction band at the interface. Clearly, such depletion potential barrier at the interface between GaAs and $In_{0.5}Ga_{0.5}As$ can affect carrier injection from QW to QD. Injected electrons confined by this potential barrier can get trapped within the QW, then these recombine with available holes inside this region and emit light. As a result, at low bias currents, as shown in figure 1(c), the QW-WL emission is greater in intensity than QD. With increasing carrier injection at higher forward bias currents, electrons can eventually cross into QD, and electroluminescence from QD increases gradually as shown in figure 1(a) and 1(b). A similar study based on such potential barrier at the interface of a heterostructure is given by Dan P Popescu *et al.* [9] and X Mu *et al.* [22] in $InAs/In_{0.15}Ga_{0.85}As/GaAs$ quantum dot-well system. P Popescu *et al.* had speculated that it can act as additional activation energy for photoluminescence other than thermal activation energy for carrier escape. Although, both of them have considered the presence of potential barriers in both conduction and valence bands due to compositionally induced strain, here we mostly focus on the effect of potential barrier in the conduction band only.

The reported conduction band offset of $In_{0.53}Ga_{0.47}As/GaAs$ is ΔE_C^{QD} ~0.43eV at 4.2K [25] while $GaAs/Al_{0.32}Ga_{0.68}As$ is ΔE_C^{QW}~0.25eV [26-28]. It is worth noting that the magnitude of band offset determines the amount of charge transferred at the interface, and hence the height of interface potential barrier. Here, we have ignored interface potential barrier, if any, between $GaAs/Al_{0.3}Ga_{0.7}As$ because we did not observe any emission from $Al_{0.3}Ga_{0.7}As$ at these currents. However, at even higher bias currents > 5 mA used for coherence studies in section 3.3, a small emission peak is observed from $Al_{0.3}Ga_{0.7}As$ at 1.85eV. Around 60% of the energy difference between band gaps of $Al_{0.3}Ga_{0.7}As$ and GaAs agrees with the reported value of ΔE_C^{QW}. However, it is interesting to note from figure 1 that the difference in the emission energy between $In_{0.5}Ga_{0.5}As$ QD and QW-WL is only ~140meV at ~8.8K indicating that the ground state energy levels of QD are quite elevated because of high gallium content and small size of QDs. The difference between the ground

state conduction band energy level of QD and top of the QD-QW potential barrier is referred as E_{loc} [29] in this report as shown in figure 2(b).

$$E_{loc} = \Delta E_c^{QD} - E_1^{QD} \quad (1)$$

where $\Delta E_c^{QD}$is conduction band offset of $In_{0.5}Ga_{0.5}As/GaAs$ and E_1^{QD} is ground state energy level of QD. This E_{loc} is strongly dependent on QD size and gallium content. This information will be used to explain thermal quenching and coherence increase in section 3.3 and 3.4, respectively.

In figure 3(a) and 3(b), we plot the variation of peak energy and FWHM of the QD electroluminescence spectra shown in figure 1 as a function of bias currents at ~8.8 K. We observed that the electroluminescence peak energy of $In_{0.5}Ga_{0.5}As$ QD slightly blue shifts with increasing applied bias. However, the variation of FWHM is not monotonic with increasing bias currents. In order to explain these findings for lower bias currents (<1 mA), it is worth pointing out that our sample is a p-i-n heterostructure and its p side is always at higher potential than n side when no bias is applied. This potential difference due to the doping difference across the device creates a built-in potential (V_{bi}) within the intrinsic layers as shown in figure 2(b). When an additional external potential (V_{ext}) is applied in the forward direction, it tries to negate [30] this built-in potential and the effective applied potential (V_{eff}) across the heterostructure is reduced as shown in equation (2).

$$V_{eff} = V_{bi} - V_{ext} \quad (2)$$

From 0.5 mA to 1 mA, the reduction of V_{eff} while increasing V_{ext} can show reverse quantum confined Stark effect (QCSE) [31]. This can result in the observed initial lowering of FWHM. QCSE in a QD can be understood as shifting of energy levels under the influence of V_{eff} within the confinement of QD. While V_{eff} is reducing under increasing forward bias, the quantum dot conduction band energy levels shift higher, and the valence band energy levels shift lower in a reversed QCSE due to a net reduction of junction electric field. This shifting of energy levels also shifts electron and holes wave function closer resulting in an increased overlap as shown in figure 2(b). This increases the emission energy but decreases the FWHM at lower bias currents. It is also clear from figure 3(b), that FWHM increases slightly at higher bias currents (> 1 mA). We further suggest that such variation of

FWHM with bias currents can be explained by a combination of QCSE and band-filling effects [32]. It is possible that QCSE is more important at lower injection currents and band-filling effects can be dominant at higher injection currents. For injection currents above 1 mA, one may also expect enhancement of Auger recombinations [33-35] within $In_{0.5}Ga_{0.5}As$ QDs as will be discussed later in section 3.3. Such increasing presence of Auger like non-radiative processes at higher bias currents can also broaden the FWHM as reported here.

Figure 4(a) and 4(b) shows the variation of spectrally integrated EL (Int. EL) of individual peaks with respect to bias current and bias voltage. The Int. EL of both QD peak and QW-WL peak increase with bias current but the rate of increase of Int. EL of QD (Int. EL_{QD}) is greater than that of QW-WL. The explanation of this behaviour has been discussed already in previous paragraphs in terms of interface potential barrier as shown in figure 2(b) and how it quantitatively affects the carrier injections and radiative recombinations from both QD and QW-WL. Also, in the inset of figure 4(a), we have plotted the difference 'Int. EL_{QW-WL} - Int. EL_{QD}' (black) and the ratio 'Int. EL_{QW-WL}/Int. EL_{QD}' (blue) to clearly indicate such variation of QW-WL and QD integrated intensities in accordance with our above explanations.

Increasing bias voltages lead to changes in both effective potential (V_{eff}) and interface potential barrier between QW and QD. In figure 4(b) we fit Int. EL_{QD} versus bias voltage to understand how applied voltage can affect the potential barrier and band alignment at the interface. Here Int. EL_{QD} is fitted with a stretched exponential function with respect to bias voltage. The reason for this empirical fit is given in the following discussion. As such, any simple relationship between current and voltage in a diode is given by Shockley diode model [36] and expressed by equation (3)

$$I(V,T) = I_0\left[\exp\left(\frac{eV}{k_BT}\right) - 1\right] \tag{3}$$

In the differential form, equation (3) can be written as,

$$\frac{dI}{dV} \propto (I + I_0) \tag{4}$$

The reverse saturation current I_0 can be mostly ignored because we are only working in forward bias and I_0 being a constant does not affect the proportionality relation in equation (4). Total sum of Int. EL from QD and QW-WL [$\Sigma(EL) = \text{Int.}\,EL_{QD} + \text{Int.}\,EL_{QW-WL}$]

increases linearly with bias current (I) as shown in the inset of figure 4(b). This indicates that $\Sigma(EL)$ is approximately proportional to bias current I in forward bias when any QD based light emitting device is operational. Therefore, assuming that the external quantum efficiency of such sample is also independent of the bias current, we replace I with the total Int. EL ($\Sigma(EL)$) in equation (4) as,

$$\frac{d\Sigma(EL)}{dV} \propto \Sigma(EL) \tag{5}$$

If similar relation is needed for Int. EL_{QD}, i.e. $\frac{d(EL_{QD})}{dV}$, then we also have to consider the contributions of Int. $EL_{QW\text{-}WL}$ towards Int. EL_{QD}. The emission coming from QW-WL has a major dependence on the interface potential barrier which controls the level of carrier injection to QD. Nevertheless, we do not know the exact relation between potential barrier and QW-WL emission. However, we understand that the potential barrier should change with bias voltage, which affects the QW-WL emission. Hence, to get the above differential relation for QD only, we need to introduce another term for such additional dependences on bias voltage. Such empirical dependence on bias voltage which is in accordance with our data can be given below as,

$$\frac{d(EL_{QD})}{dV} \propto (EL_{QD})/V^n \tag{6}$$

Putting the constant of proportionality in equation (6) as α gives,

$$\frac{d(EL_{QD})}{dV} = \alpha EL_{QD}/V^n \tag{7}$$

Finally solving the differential equation (7), we get the stretched exponential form of that empirical dependence as,

$$EL_{QD} = A.\exp(\frac{-\alpha}{mV^m}) \tag{8}$$

Here, A is constant of integration and m = (n+1). We believe that α has inverse temperature dependence. Since the curve fitting is done at a constant temperature (~8.8 K) and only the bias is varied, the exact temperature dependence cannot be extracted from this relationship. The estimates obtained from the curve fitting of equation (8) are A = 1482 ± 72 a.u., α = 365 ± 28 a.u. and m = 5.6 ± 0.1, respectively. Such stretched exponential dependence may be

indicative of the presence of energy dispersive and bias dependent rate processes within the heterostructure.

For further understanding of the effective role of the potential barrier at the $In_{0.5}Ga_{0.5}As/GaAs$ interface in confining the carriers undergoing radiative recombination in either QD or in QW-WL, we fit a log-log plot of Int. EL vs. bias current of QD and QW-WL at ~8.8 K as shown in figure 4(c). The power law exponent for Int. EL_{QD} is found to be 1.73±0.02. For Int. $EL_{QW\text{-}WL}$, this exponent is 0.78±0.02. This exponent value around unity is possibly connected to the presence of excitonic recombinations in the QW-WL layers. Clearly, more carriers are being effectively recombined inside QDs as compared to QW-WL. We have already explained that Int. EL_{QD} depends upon the bias current that incorporates the effect of potential barrier. After a particular applied bias, the carrier jumps into QD from QW after crossing that barrier and carrier transport in QDs increases exponentially. The exponent value ~2 in case of QD indicates that EL intensity is increasing in QDs faster than that of QWs with increasing bias current. Usually, such large exponent points to bi-molecular recombination of free electrons and holes. However, all charge carriers inside these QDs are quantum confined from all three spatial directions. Therefore, we tend to attribute this higher exponent value (~2) to the symptomatic presence of trions or biexcitons related with radiative recombination in QDs [37]. Such evidences of the presence of trions or biexcitons may also point towards likelihood of non-radiative Auger recombination of these excitonic complexes [34] and how it is broadening the EL peaks in figure 3(b) at higher bias currents. Further details of these understandings will be discussed again in section 3.3.

3.2 Temperature dependence of electroluminescence from QD and QW-WL

Figure 5(a) shows EL spectra at different temperatures under a constant bias current of ~2.2 mA. At such high current, a significant number of carriers can easily cross the interface potential barriers between QW-WL and QD, and finally get trapped inside the QDs. Hence, we expect no significant contribution from this interface potential barrier over the investigated temperature range. However, any QD-based light emitting devices operating at lower threshold currents, this barrier can play a decisive role. EL from QW-WL is visible from ~8.8 K to 200 K, while the QD emission is detected up to 300K, which is also depicted as colour coded contour plot in figure 5(b). The main reason for emission quenching in case of QD as well as QW-WL are thermal escape of charge carriers and activation of non-

radiative defects states at high temperatures. The potential energy barrier for carrier escape in case of QD is E_{loc}~140 meV, while in the case of QW-WL, it is band offset at GaAs/$Al_{0.3}Ga_{0.7}As$ ΔE_C^{QW}~250 meV. Despite a smaller potential energy barrier, the QD emission is still detectable up to 300K because the QDs have strong spatial confinement of charge carriers leading to increased probability of electron-hole recombinations. Moreover, the QD ground state also provides the lowest energy for the system of injected carriers. In case of QW-WL, carriers escape to $Al_{0.3}Ga_{0.7}As$ barrier layer and are swept away from the active region to become irrelevant for EL in this spectral range. Therefore, even after receiving some escaped carriers from QD, non-radiative recombination and thermal escape can collectively dominate over radiative recombinations leading to significant emission quenching in QW-WL. As a result, the QW-WL peak is nearly non-existent above 200K.

The peak energy of QDs is also red shifted with increasing temperatures. Variation of QD peak energy is fitted with three models, namely Varshni [38], Vina *et al.* [39], and Passler [40] as shown in figure 6. The fitted parameters are given in Table 1. Previously, it was shown that the behaviour of the peak energy of QDs with respect to temperature is sigmoidal [10, 17]. In some of these previous studies, the measured peak energy actually red shifts more than that predicted using Varshni fitting after a particular temperature. This effect was attributed to redistribution of charge carriers among QDs, where charge carriers get transferred into bigger QDs with lower emission energy. However, in our case, no such sigmoidal variation of peak energy is observed with increasing temperature. This is possible if there are no effective channels of carrier redistribution between the QDs either through wetting layer or QW even though the thermal escape of carriers from QDs is possible at higher temperatures.

Table 1. Fitted parameter of Varshni, Vina *et al.* and Passler model for peak energy of QD

Models:	Varshni	Passler	Vina *et al.*
	$E(T) = E(0) - \frac{\alpha T^2}{\beta + T}$	$E(T) = E(0) - \frac{\alpha\theta}{2}\left(\sqrt[4]{1 + \frac{\pi^2}{6}\left(\frac{2T}{\theta}\right)^2 + \left(\frac{2T}{\theta}\right)^4} - 1\right)$	$E(T) = a - b\left(1 + \frac{2}{e^{\frac{\theta}{T}} - 1}\right)$
E(0) (eV)	1.338	1.338	a = 1.361 ± 0.003 eV
10^{-4} α (eV/K)	3.0 ± 0.5	2.4 ± 0.2	b=0.023 ± 0.004 eV
β or θ (K)	β = 230 ± 87	θ = 205 ± 47	θ =300 ± 36

In figure 7(a) and 7(b), the Int. EL_{QD} and Int. $EL_{QW\text{-}WL}$ are plotted as a function of inverse of sample temperature (1/T), respectively, and fitted using Arrhenius equations (9) of EL quenching with only a single activation energy. The effective free energy barrier is given by:

$$I(T) = \frac{I_0}{1+A.exp\left(-\frac{E_a}{k_B T}\right)} \tag{9}$$

where k_B is the Boltzman constant, I_0 is integrated EL at 8.8 K, E_a is the activation energy, and A is a pre-exponential factor. E_a and A are fitting parameters and are given in Table 2. Although, the activation energies required for EL quenching from QD and QW-WL are well below the respective potential energy barriers, E_{loc} and ΔE_C^{QW}, the thermal escape of charge carriers is still possible. This is because of the existence of thermodynamically non-zero probability of carrier escape, i.e. ~exp($^{-E_a}/_{k_B T}$) from such potential wells. A model is given in figure 7(c) indicating all such carrier dynamics. These can be both radiative and non-radiative recombinations inside the QD and the QW. Here we assume that these fitted activation energies for both peaks are not only just thermal activation energies for carrier escape from QDs and QWs, but also these include the combined effects of activation of thermal escape as well as non-radiative recombinations through defects.

Table 2. Fitted values of Arrhenius equations (9) for QD and QW-WL, respectively

For QD	*For QW-WL*
E_a = 21 ± 4 meV	E_a= 52 ± 10 meV
A = 25 ± 14	A = 201 ± 192

3.3. Bias and temperature effects on optical coherence

In the previous sections we reported EL from sample A under bias currents from 0.11 mA to 2.2 mA. Here, we will present measurements of temporal coherence of EL of QDs and QW-WL at even higher biases up to 15mA. For these, we have used basic Michelson Interferometry to measure first order autocorrelation function $g^{(1)}(\tau=0)$ as described in section 2. The modulus of $g^{(1)}(\tau=0)$ can be directly calculated from the visibility of interference pattern generated by the Michelson interferometer [41] using equation (10). In figure 8(a) and

8(b), $g^{(1)}(\tau=0)$ of spectrally separated EL emissions from QDs and QW-WL at different bias currents and temperatures are shown, respectively.

$$\left| g^{(1)}(\tau = 0) \right| = Visiblity = \frac{I_{max} - I_{min}}{I_{max} + I_{min}} \quad (10)$$

Here I_{max} and I_{min} are the maxima and minima of fringes in recorded Michelson interference pattern. In figure 8(a), we see that $g^{(1)}(\tau=0)$ of QDs decreases with increasing bias current while for QW-WL, it is increasing. The decrease of $g^{(1)}(\tau=0)$ in case of QDs likely due to Auger recombinations (AR) within these QDs at such high bias currents. AR is a non-radiative process usually significant at high carrier densities and in low bandgap materials. AR is effective in suppressing luminescence and reducing temporal coherence at higher injection currents for QD EL. From figure 4(c) it is clear that the Integrated EL of QD already begins to saturate above bias currents of ~1 mA. EL spectra at such higher bias currents are not shown. Interestingly, the presence of Auger process can be confirmed here mainly on the basis of the observed differences in temporal coherence of QDs EL and QW-WL EL. This is because, contrary to QDs, QW EL is not affected by AR mainly because of the following reasons. First, the QW recombinations only occur from remaining carriers in QW-WL, whose density is comparatively smaller than that of QDs. This can be understood from the EL of QDs and QW-WL shown in figure 4(a) where EL of QDs exceeds EL of QW-WL at around 2mA. Secondly, QWs has a higher band gap than QDs [34, 42-44]. Thirdly, QWs has a lesser spatial confinement than QDs which also keeps the carrier density below the threshold for any significant Auger process. Therefore, the temporal coherence of QW-WL EL still increases with increasing bias currents in the absence of any significant AR process within QW-WL.

Auger is a three particle scattering process where either two electrons and one hole or two holes and one electron ($e^-e^-h^+$ or $h^+h^+e^-$) get involved to recombine non-radiatively. The recombination energy of e^- and h^+, instead of getting emitted as photon, is provided to a third particle which transfers to higher available energy states resulting in a final overall non-radiative recombination process. During AR process in QDs, the third charge carrier carrying the recombination energy can also undergo transfer from the QD to the QW levels. This type of non-radiative AR recombination can destroy temporal phase correlation between emitted photons leading to a reduced $g^{(1)}(\tau=0)$ in QDs. Also, we already attributed the power law exponent of Integrated EL with bias currents to the presence of trions or biexcitons in these QDs in section 3.1. This explanation agrees with the discussion provided by Kurzmann *et al.*

[34] for InAs/GaAs QD at 4.2 K where they concluded that trions can effectively contribute to AR.

Observed variations of temporal coherence with temperature at a bias current of 15 mA are shown in figure 8(b). These indicate interesting comparison between QD EL and QW-WL EL. With increasing temperature, the coherence of QDs increases despite the increase in thermal energy of charge carriers and then it saturates. Due to small E_{loc} in QDs, the charge carriers easily escape QDs with increasing temperatures. This can significantly lower the carrier density below the required AR threshold inside these QDs. As a result of this effective reduction of carrier density at higher temperatures, there can be subsequent decrease of Auger recombination [45, 46] leading to an increase of coherence of QD EL with increasing temperatures up to a certain level and nearly saturates. However, the $g^{(1)}(\tau=0)$ for QW-WL emissions are not affected, as expected, due to the absence of any significant Auger process at higher temperatures. As a result, the optical coherence of QW-WL EL mostly decreases above 50 K with usual increase in non-radiative recombinations with increasing temperatures. EL intensity of QW-WL at temperatures higher than ~120 K is small enough to get any reasonable estimate of $g^{(1)}(\tau=0)$.

To the best of our knowledge, there are not any literature reports that had related coherence of electroluminescence with Auger recombination in QDs. Moreover, here we showed an interesting interplay between two effects: electroluminescence quenching and temporal coherence of electroluminescence due to the escape of charge carriers from QDs with increasing temperatures. On one hand, charge depopulation from QDs results in quenching of QD EL with increasing temperatures. On the other hand, due to reduced charge carrier density, the ongoing Auger recombination also reduces which results in more coherent light emission at higher temperatures. In a way, spectrally selective measurements of temporal coherence could be considered as a useful method to sense the presence of AR. From the point of view of applications, this sensitivity of $g^{(1)}(\tau=0)$ to detect AR and the above mentioned interplay between quenching and temporal coherence of electroluminescence can be suitable in optimizing quantum dots based light emitting devices.

3.4. Experimental Results on Sample B with DBR

We also investigated sample B, which has a structure similar to a vertical cavity surface emitting laser (VCSEL) that include QDs in the active region and DBR stacks on both sides, under similar electrical biases and temperatures. Clearly, the EL peaks of QDs and QW-WL are distinct and well separated in comparison to sample A as shown in figure 9(a) and 9(b). The spectral evolution of peaks with increasing biases at low temperature (~10 K) is still the same as Sample A, which indicates the presence of potential barrier at the interface of QDs and QW. Although the peak position of QDs in sample B is the same as for sample A, the emission peaks in sample B are narrower. The FWHM in sample A ranges from 42 meV to 48 meV while in sample B, it saturates to a much smaller maximum value ~30meV. This can be explained by the presence of DBR stacks at both ends of the structure, which forms an optical cavity. So, we attribute the observed reduction in the emission broadening to the selective nature of 1D photonic band gap within such DBR stacks. In sample B, we also observe that the peaks follow similar trends with temperature. However, the QW-WL peak disappears nearly at 250 K instead of 200 K as observed in sample A. Due to three layers of QDs-QWs instead of six as in Sample A, there can be twice the amount of injected charge carrier densities in the active region of sample B. This could be the reason behind non-vanishing of QW-WL EL even at 250 K for Sample B.

4. Conclusion

We conclude that the interface potential barrier between QDs and QWs has an important role in determining carrier dynamics inside $In_{0.5}Ga_{0.5}As/GaAs/Al_{0.3}Ga_{0.7}As$ QD-QW heterostructure. For device applications, in low current regime, this barrier could play a more decisive role. We further found an empirical dependence of EL of QDs on applied bias voltage, which directly incorporates the effect of the same interface potential barrier. Temperature dependence of electroluminescence spectra shows that thermal escape of injected charge carriers and their non-radiative recombinations are the main causes of EL quenching. We also performed temporal coherence measurements and argued that Auger recombination is a major source for loss of coherence in QDs emission at high carrier densities. With increasing temperatures, due to the escape of carriers from QDs, charge density reduces resulting in reduced Auger recombinations at a fixed bias current. These reduced Auger recombinations then further enhance the first order temporal correlation of

light emission. Therefore, depopulation of carriers from QDs results in lower EL but with improved optical coherence at higher temperatures.

In fact, we even argued that measurement of temporal coherence of individual spectral peaks could be an important sensitive tool to detect the presence of Auger recombinations in QDs. All these results also indicate that by using proper materials and device engineering of potential barriers within such QDs heterostructure, a dynamical balance can be found between thermally activated loss of carriers which do not recombine radiatively and the fraction of injected carriers which produce electroluminescence. Therefore, this work demonstrated how such interface potential barrier mediated charge transfers to and from QDs help to maintain the crucial interplay between electroluminescence quenching and temporal coherence of electroluminescence. Such optimisations will be important to control not only the strength, but also the coherence of electroluminescence resulting in an efficient QDs based light emitting devices for lasing.

ACKNOWLEDGRMENTS

SD acknowledges Department of Science and Technology, India (Research Grants # SR/S2/CMP-72/2012 and SR/NM/TP13/2016). MKS is thankful to IISER-Pune for Integrated PhD and PhD Fellowship and AB is thankful to DST, India for Inspire PhD Fellowship, respectively. YGG acknowledges the financial support from the Brazilian agency Fundação de Amparo a Pesquisa do Estado de São Paulo (FAPESP) (Research Grant # 16/10668-7 and 18/01808-5). MH acknowledges support from the UK Engineering and Physical Sciences Research Council.

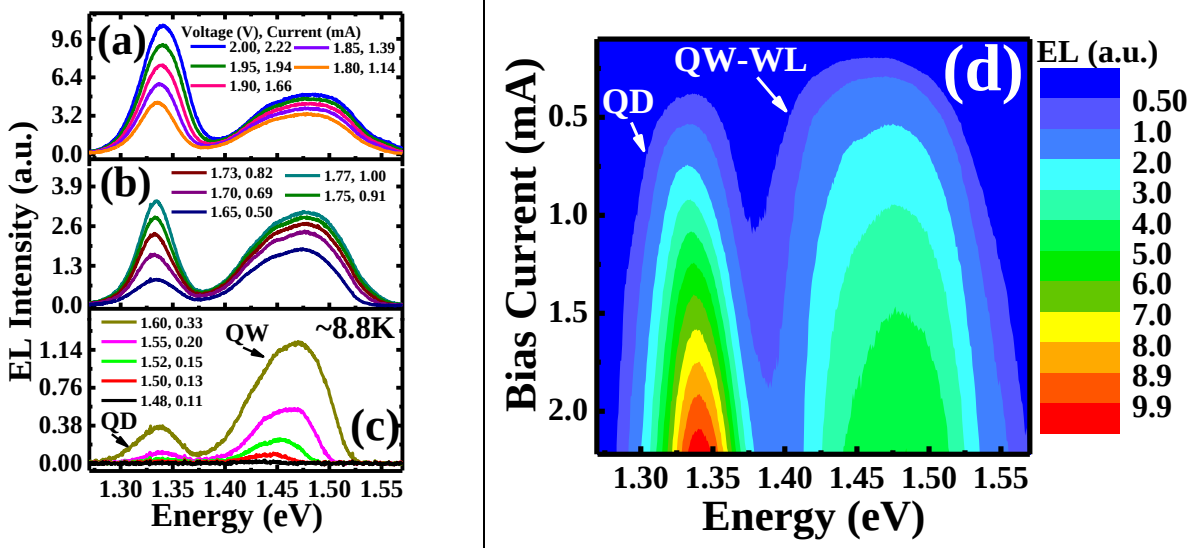

Figure 1. (a), (b), (c) Electroluminescence (EL) spectra of $In_{0.5}Ga_{0.5}As/GaAs/Al_{0.3}Ga_{0.7}As$ quantum dot-quantum well (QD-QW) heterostructure (sample A) at ~8.8 K under decreasing levels of forward bias voltage and corresponding bias currents, respectively. (d) 2D Contour plot of the same spectra with colour coded EL intensity at different bias currents. Emission around 1.33 eV is from QD while broad emission of QW and WL is around 1.47 eV. Initial emission from QW-WL at low bias current is dominated by emissions from QDs at higher currents.

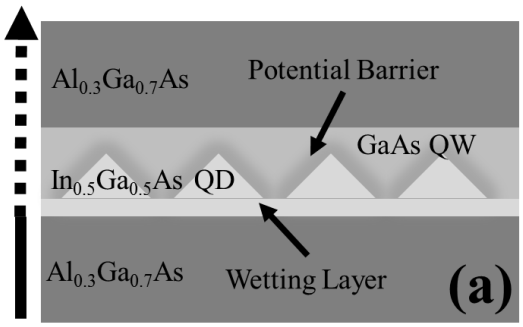

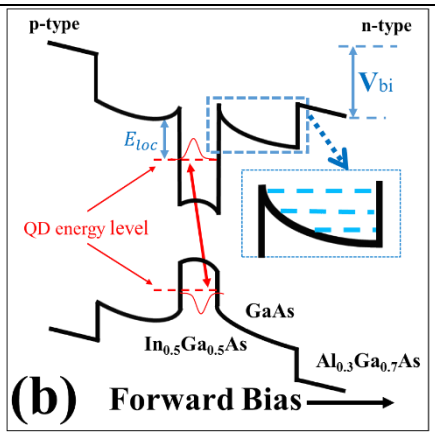

Figure 2. (a) Schematic diagram of the sample(s). The light grey triangles are self-assembled $In_{0.5}Ga_{0.5}As$ QDs over the wetting layer (light grey). The QDs are grown inside GaAs/$Al_{0.3}Ga_{0.7}As$ QW. The grey shadow over QDs represents the potential barrier which prevents the carrier injection. Dotted arrow on left shows the repetition of same structure along the growth direction. Sample A has six layers of QD-QWs while Sample B has three layers of QD-QWs only. (b) Schematic band diagram of $In_{0.5}Ga_{0.5}As$/GaAs/$Al_{0.3}Ga_{0.7}As$ QD-QW heterostructure. The direction of the applied forward bias is given by the black arrow. Quantized energy levels (blue) of QW within the potential barrier at the interface of QDs and QW are shown in the inset. Potential barrier at GaAs/$Al_{0.3}Ga_{0.7}As$ interface and wetting layers are omitted from this schematic band diagram for simplicity.

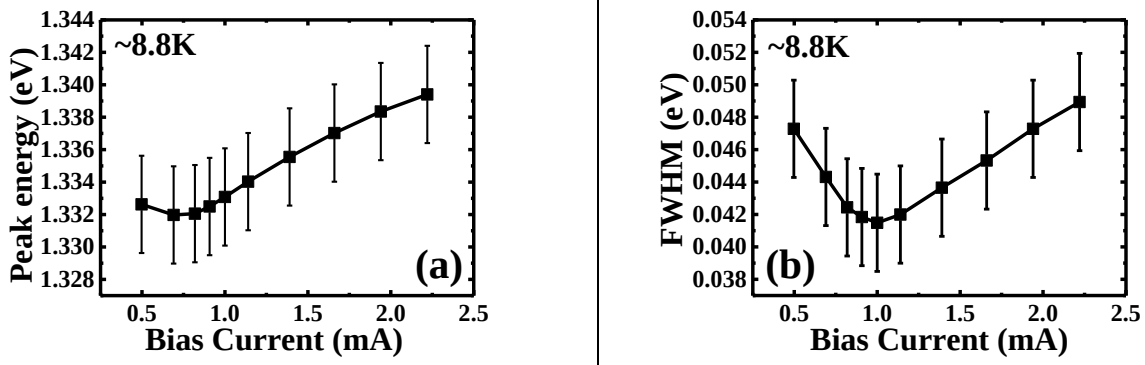

Figure 3. (a) Peak energy and (b) FWHM of EL spectra of $In_{0.5}Ga_{0.5}As$ QD at ~8.8K are plotted respectively as function of bias currents. The error bars in both plots indicate combined contributions from experimental bandwidth ($\Delta E \sim 3meV$) at the peak wavelength and the errors due to fitting Gaussian line shapes to each peak.

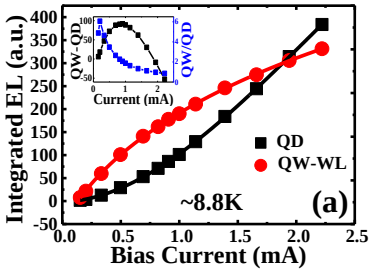

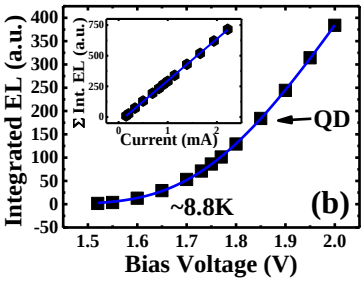

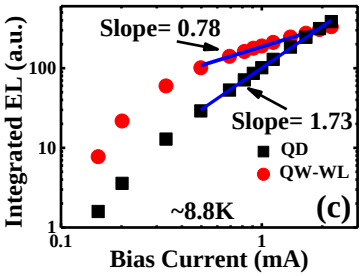

Figure 4. (a) Integrated EL of the QDs and the QW-WL peak from figure 1 as function of bias current. The inset shows the difference of Integrated EL of QW-WL and QD (as QW-QD with black dots) which has a maximum around 1 mA. It also shows the ratio of Integrated EL of QW-WL and QD (as QW/QD with blue dots) which is mostly decreasing with bias current. All lines are guide for the eyes only. (b) Integrated EL of QD is fitted against bias voltage. It indicates voltage activated increase of EL with increasing forward bias. Inset of (b) shows linear increase of total Integrated EL of QW-WL and QD with bias current. (c) Integrated EL of QW-WL and that of QDs are plotted against bias currents in log-log scale. The plots are fitted with straight lines (blue) at higher currents. Estimated slopes of QW-WL EL and QD EL are 0.78 and 1.73, respectively.

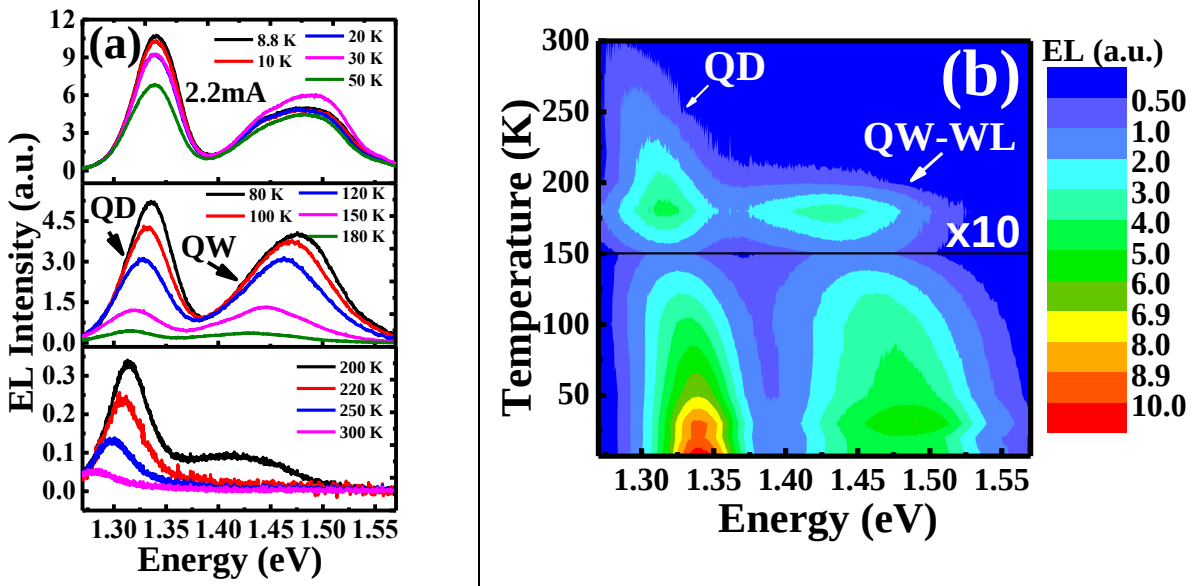

Figure 5. (a) EL spectra at constant bias current ~2.2 mA for different temperatures (b) 2D colour coded contour plot of the same spectra at different temperatures. The QW-WL peak vanishes above ~200 K. There is a red shift in peak energy of QDs with increasing temperature.

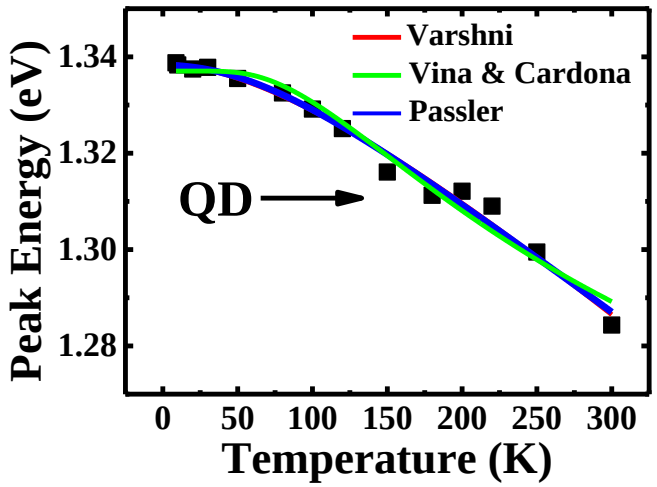

Figure 6. Peak energy of QDs emission as function of temperature (black square). The plot is fitted with Varshni (Red), Vina *et al*. (Green), Passler (Blue) models of semiconductor band-gap variation with respect to temperature.

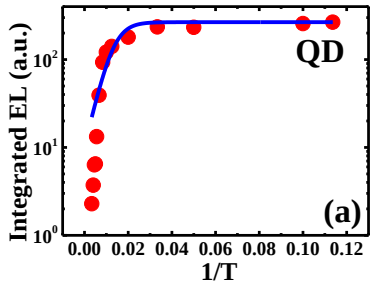

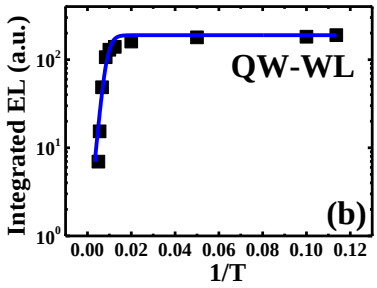

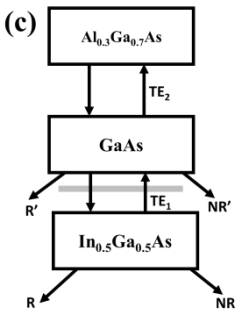

Figure 7. Integrated EL of (a) QDs and (b) QW-WL are plotted with respect to inverse of temperature in K^{-1}, respectively. The plots are fitted with Arrhenius formula of luminescence quenching with single activation energy. (c) Schematic diagram for radiative and non-radiative transitions in $In_{0.5}Ga_{0.5}As$/GaAs QD and GaAs/$Al_{0.3}Ga_{0.7}As$ QW. R and R', and NR' and NR are radiative recombination and non-radiative recombination of QDs and QWs, respectively. Downward arrows indicate the carrier capture while upward arrow shows the thermal escape (TE). TE_1 shows escape for carrier from $In_{0.5}Ga_{0.5}As$ QD to GaAs and TE_2 is carrier escape from GaAs QW to $Al_{0.3}Ga_{0.7}As$ barrier layer. The grey line between QDs and QW represents the presence of interface potential barrier restricting the carriers from entering the QD at low injection currents.

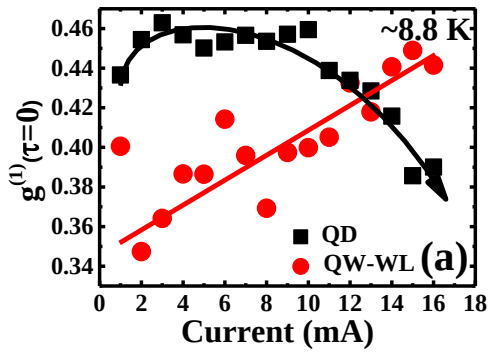

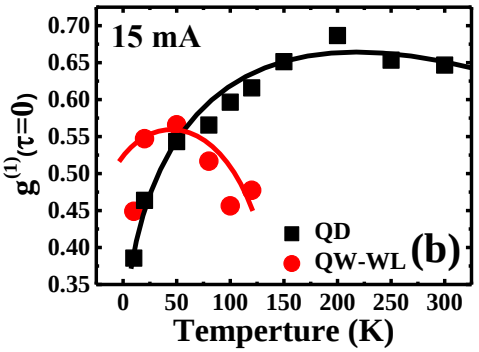

Figure 8. First order correlation function, $g^{(1)}(\tau=0)$ are estimated for both EL of QD and EL of QW-WL, respectively. These $g^{(1)}(\tau=0)$ are plotted against bias currents at ~8.8 K in (a) and against temperatures at a fixed bias current of 15 mA in (b), respectively. All lines in (a) and (b) are guide for the eyes only. Auger recombination is possibly weakening the optical coherence at such high currents. However, thermal escape of charge carriers from QDs results in reduced carrier density at higher temperatures. This suppresses Auger recombination, which shows up as an increase of temporal coherence of QD EL at higher temperatures.

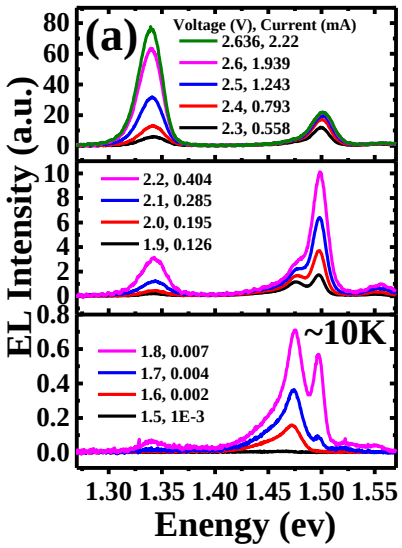

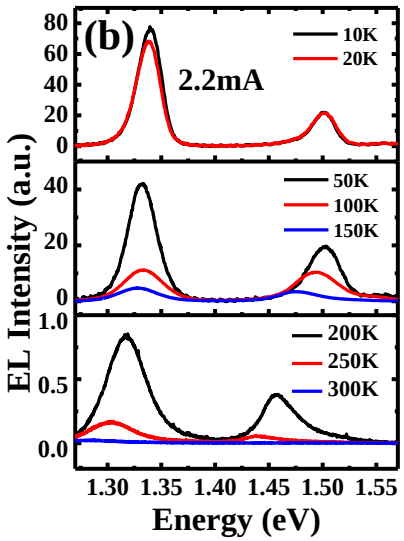

Figure 9. (a) EL spectra at different applied biases and corrosponding bias currents of Sample B with DBR stacks. (b) EL spectra at different temperatures with fixed bias current of ~2.2 mA. Here the emisions from both QDs and QW-WL are much sharper in comparison with Sample A.

References

[1] Grundmann M and Bimberg D 1997 Gain and Threshold of Quantum Dot Laser: Theory and Comparison to Experiment *Jpn. J. Appl. Phys*. **36** 4181-4187

[2] Reithmaier J P and Forchel A 2003 Recent advances in semiconductor quantum-dot lasers *C R Phys* **4** 611-619

[3] Schäfer F, Reithmaier J P and Forchel A 1999 High-performance GaInAs/GaAs quantum-dot lasers based on a single active layer *Appl. Phys. Lett.* **74** 2915

[4] Liu G T, Stintz A, Li H, Malloy K J and Lester L F 1999 Extremely low room-temperature threshold current density diode lasers using InAs dots in $In_{0.15}Ga_{0.85}As$ quantum well *Electron. Lett.* **35** 1163-1165

[5] Park G, Shchekin O B, Huffaker D L and Deppe D G 2000 InGaAs quantum dot lasers with sub-milliamp thresholds and ultra-low threshold current density below room temperature *Electron. Lett.* **36** 1283-1284

[6] Kondow M, Uomi K, Niwa A, Kitatani T, Watahiki S and Yazawa Y 1996 GaInNAs: A Novel Material for Long-Wavelength Range Laser Diodes with Excellent High Temperature Performance *Jpn. J. Appl. Phys*. **35** 1273

[7] Lott J A, Ledentsov N N, Ustinov V M, Maleev N A, Zhukov A E, Kovsh A R, Maximov M V, Volovik B V, Alferov Zh I and Bimberg D 2000 InAs-InGaAs quantum dot VCSELs on GaAs substrates emitting at 1.3 μm *Electron. Lett.* **36** 1384-1385

[8] Shoji H, Mukai K, Ohtsuka N, Sugawara M, Uchida T and Ishikawa H 1995 Lasing at Three-Dimensionally Quantum-Confined Sublevel of Self-organized $In_{0.5}Ga_{0.5}As$ Quantum Dots by Current Injection *IEEE Photon. Technol. Lett*. **7** 1385-1387

[9] Popescu D P, Eliseev P G, Stintz A and Malloy K J 2004 Temperature dependence of the photoluminescence emission from InAs quantum dots in a strained $Ga_{0.85}In_{0.15}As$ quantum well *Semicond. Sci. Technol.* **19** 33-38

[10] Torchynska T V, Casas Espinola J L, Borkovska L V, Ostapenko S, Dybiec M, Polupan O, Korsunska N O, Stintz A, Eliseev P G and Malloy K J 2007 Thermal activation of excitons in asymmetric InAs dots-in-a-well $In_xGa_{1-x}As$/GaAs structures *J. Appl. Phys.* **101** 024323

[11] Maksimov M V *et al.* 1997 Quantum dot injection heterolaser with ultrahigh thermal stability of the threshold current up to 50 °C *Semiconductors* **31** 124

[12] Maksimov M V *et al.* 1997 InGaAs/GaAs Quantum Dot Lasers with Ultrahigh Characteristic Temperature (T_0= 385 K) Grown by Metal Organic Chemical Vapour Deposition *Jpn. J. Appl. Phys.* **36** 4221

[13] Shoji H, Nakata Y, Mukai K, Sugiyama Y, Sugawara M, Yokoyama N and Ishikawa H 1997 Temperature dependent lasing characteristics of multi-stacked quantum dot lasers *Appl. Phys. Lett.* **71** 193

[14] Sabaeian M and Khaledi-Nasab A 2012 Size-dependent intersubband optical properties of dome-shaped InAs/GaAs quantum dots with wetting layer *Appl. Opt.* **51** 4176-4185

[15] Kioupakis E, Yan Q, Steiauf D and Van de Walle C G 2013 Temperature and carrier-density dependence of Auger and radiative recombination in nitride optoelectronic devices *New J. Phys.* **15** 125006

[16] Fang Y *et al.* 2015 Investigation of temperature dependent photoluminescence in multi-quantum wells *Sci. Rep.* **5** 12718

[17] Sanguinetti S, Henini M, Alessi M G, Capizzi M, Fringeri P and Franchi S 1999 Carrier thermal escape and retrapping in self-assembled quantum dots *Phys. Rev. B* **60** 8276

[18] Klimov V I, Mikhailovsky A A, McBranch D W, Leatherdale C A and Bawendi M G 2000 Quantization of Multiparticle Auger Rates in Semiconductor Quantum Dots *Science* **287** 1011

[19] Piprek J 2010 Efficiency droop in nitride-based light-emitting diodes *Phys. Status Solidi* A **207** 2217–2225

[20] Bhunia A, Bansal K, Henini M, Alshammari M S and Datta S 2016 Negative activation energy and dielectric signatures of excitons and excitonic Mott transitions in quantum confined laser structures *J. App. Phys.* **120** 144304

[21] Bansal K and Datta S 2011 Voltage modulated electro-luminescence spectroscopy to understand negative capacitance and the role of sub-bandgap states in light emitting devices *J. App. Phys.* **110** 114509

[22] Mu X, Ding Y J, Hopkinson M 2007 Dynamics of Carriers Photogenerated in a Dot-in-a-Well Nanostructure *Laser Phys.* **17** 305–309

[23] Bansal K and Datta S 2013 Temperature dependent reversal of voltage modulated light emission and negative capacitance in AlGaInP based multi quantum well light emitting devices *Appl. Phys. Lett.* **102** 053508

[24] Lindell A, Pessa M, Salokatve A, Bernardini F, Nieminen R M and Paalanen M 1997 Band offsets at the GaInP/GaAs heterojunction *J. Appl. Phys.* **82** 3374 (1997)

[25] Yahyaoui M, Sellami K, Boujdaria K, Chamarro M and Testelin C 2013 Band parameters of InGaAs/GaAs quantum dots: electronic properties study *Semicond. Sci. Technol*. **28** 125018

[26] Pfeiffer L, Schubert E F, West K W and Magee C W 1991 Si dopant migration and the AlGaAs/GaAs inverted interface *Appl. Phys. Lett*. **58** 2258

[27] Menéndez J, Pinczuk A, Werder D J, Gossard A C and English J H 1986 Light scattering determination of band offsets in GaAs-$Al_xGa_{1-x}As$ quantum wells *Phys. Rev. B* **33** 8863

[28] Koteles E S 1993 Determining energy-band offsets in quantum wells using only spectroscopic data *J. App. Phys.* **73** 8480

[29] Bimberg D, Grundmann M and Ledentsov N N 1998 *Quantum Dot Heretostructures* (New York: Wiley) p 155

[30] Sze S M 2007 *Physics of semiconductor devices* (Wiley Second edition) p 75

[31] Chen H, Liu Z H, Shih P, Su C, Chen C, Lin C, Yao Y, Kiang Y, Yang C 2014 Independent variations of applied voltage and injection current for controlling the quantum-confined Stark effect in an InGaN/GaN quantum-well light-emitting diode *Opt. Express* **22** 8367-8375

[32] Wang H, Ji Z, Qu S, Wang G, Jiang Y, Liu B, Xu X and Mino H 2012 Influence of excitation power and temperature on photoluminescence in InGaN/GaN multiple quantum wells *Opt. Express* **20** 3932-3940

[33] Nilsson H H, Zhang J Z and Galbraith I 2007 Enhancement and reduction of line broadening due to Auger scattering in modulation-doped InGaAs/GaAs quantum dot devices *Appl. Phys. Lett.* **91** 161113

[34] Kurzmann A, Ludwig A, Wieck A D and Lorke and Geller M 2016 Auger Recombination in Self-Assembled Quantum Dots: Quenching and Broadening of the Charged Exciton Transition *Nano Lett.* **16** 3367−3372

[35] Nilsson H H, Zhang J Z and Galbraith I 2005 Homogeneous broadening in quantum dots due to Auger scattering with wetting layer carriers *Phys. Rev. B* **72** 205331

[36] Shockley W 1949 The theory of p–n junctions in semiconductors and p–n junction transistors. *Bell Syst. Tech. J.* **28** 435–489

[37] Nobrega J A, Gordo V O, Galeti H V A, Gobato Y G, Brasil M J S P, Taylor D, Orlita M and Henini M 2015 Spin polarization of carriers in resonant tunneling devices containing InAs self-assembled quantum dots *Superlat. Microst.* **88** 574-581

[38] Varshni Y P 1967 Temperature dependence of the energy gap in semiconductors *Physica (Amsterdam)* **34** 149

[39] Vina L, Logothetidis S and Cardona M 1984 Temperature dependence of the dielectric function of germanium *Phys. Rev. B* **30** 1979

[40] Pässler R 1998 Dispersion-related assessments of temperature dependences for the fundamental band gap of hexagonal GaN *J. Appl. Phys.* **83** 3356

[41] Fox M 2006 *Quantum Optics: An Introduction* 2006 (New York: Oxford University Press) p 19

[42] Aytac Y, Olson B V, Kim J K, Shaner E A, Hawkins S D, Klem J F, Olesberg J, Flatte M E, and Boggess T F 2016 Bandgap and temperature dependence of Auger recombination in InAs/InAsSb type-II superlattices *J. Appl. Phys.* **119** 215705

[43] Robel I, Gresback R, Kortshagen U, Schaller R D and Klimov V I 2009 Universal Size-Dependent Trend in Auger Recombination in Direct-Gap and Indirect- Gap Semiconductor Nanocrystals *Phys. Rev. Lett.* **102** 177404

[44] Pietryga J M, Zhuravlev K K, Whitehead M, Klimov V I and Richard D. Schaller 2008 Evidence for Barrierless Auger Recombination in PbSe Nanocrystals: A Pressure-Dependent Study of Transient Optical Absorption *Phys. Rev. Lett.* **101** 217401

[45] Ghosh S, Bhattacharya P, Stoner E, Singh J, Jiang H, Nuttinck S and Laskar J 2001 Temperature-dependent measurement of Auger recombination in self- organized $In_{0.4}Ga_{0.6}As$/GaAs quantum dots *Appl. Phys. Lett.* **79** 722

[46] Narvaez G A, Bester G and Zunger A 2006 Carrier relaxation mechanisms in self-assembled (In,Ga)As/GaAs quantum dots: Efficient P→S Auger relaxation of electrons *Phy. Rev. B* **74** 075403